Journal of Archaeological Science 62 (2015) 128–142

Contents lists available at ScienceDirect

Journal of Archaeological Science

journal homepage: http://www.elsevier.com/locate/jas

Micro-photogrammetric characterization of cut marks on bones

Miguel Ángel Maté González [a], José Yravedra [b, *], Diego González-Aguilera [a], Juan Francisco Palomeque-González [b], Manuel Domínguez-Rodrigo [b, c]

[a] Department of Cartography and Terrain Engineering, Polytechnic School of Avila, University of Salamanca, Hornos Caleros 50, 05003 Avila, Spain
[b] Department of Prehistory, Complutense University, Prof. Aranguren s/n, 28040 Madrid, Spain
[c] IDEA (Institute of Evolution in Africa), Museo de los Orígenes, Plaza de San Andrés 2, 28005 Madrid, Spain

ARTICLE INFO

Article history:
Received 1 June 2015
Received in revised form
3 August 2015
Accepted 4 August 2015
Available online 6 August 2015

Keywords:
Taphonomy
Cut marks
Macro-photogrammetry
Computer vision
Image-based modelling

ABSTRACT

In the last few years, the study of cut marks on bone surfaces has become fundamental for the interpretation of archaeological sites and prehistoric butchery practices. Due to the difficulties in the correct identification of cut marks, many criteria for their description and classifications were suggested. This article presents an innovative methodology which supplements the microscopic study of cut marks. Despite the benefits of using scanning electron microscopy (SEM) for the two-dimensional identification of these marks, it has a number of drawbacks such as the high costs and, consequently, the limited sample studied. In this article, a low-cost technique for the analysis of cut mark micromorphology from a tri-dimensional perspective is introduced. It provides a high-resolution approach to cut mark characterisation such as morphology, depth, width, and angle estimation as well as section determination, measured directly on the marks on bones. Macro-photogrammetry records quantitative and qualitative information which can be statistically processed with standard multivariate and geometric morphometric tools.

1. Introduction

Lartet (1860), Peale (1870), Lartet and Christy (1875) and Martin (1909) were pioneers in the study of cut marks in the late 19th and early 20th centuries. They observed the presence of marks in archaeological assemblages, but did not engage into any fine-detailed analysis of them. During the 20th century, several scholars observed, classified and described cut marks, amongst which the seminal studies by White (1952, 1953, 1954, 1955), Binford (1981), Bunn (1982) or Shipman (1981) should be emphasized. In the last few years, the analysis of cut marks has become extremely relevant in the interpretation of the archaeological record, as it has offered evidence to interpret such diverse behaviours as hunting by Olduvai hominins 1.8 Myr ago (Bunn and Kroll, 1986; Domínguez-Rodrigo et al., 2007), or the replacement of lithic butchery tools by metal ones during the Holocene (Greenfield, 1999, 2004).

In the past 20 years, cut mark analysis has become more sophisticated. Experimental recreation of cut mark frequencies and their anatomical location on ungulate carcasses were considered (Capaldo, 1997; Domínguez-Rodrigo, 1997), as well as replications of different butchery processes such as filleting, dismembering or evisceration (Binford, 1981; Lyman, 1987; Nilsen, 2001; Galán and Domínguez-Rodrigo, 2013). Others studies focused on discriminating cut marks from other processes such as trampling (Shipman, 1981; Shipman and Rose, 1983; Behrensmeyer et al., 1986; Domínguez-Rodrigo et al., 2009), or characterizing the raw material of the cutting tool: flint, obsidian, metal, quartz (Olsen, 1988; Greenfield, 1999, 2004, 2006a, b; Bello and Soligo, 2008; Yravedra et al., 2009), shell (Choi and Driwantoro, 2007), or bamboo (Spennerman, 1990; West and Louys, 2007). Other research addressed cut mark morphology according to stone tool type (i.e. simple or retouched flakes, handaxes) (Walker, 1978; Shipman and Rose, 1983; Bello et al., 2009; Domínguez-Rodrigo et al., 2009; De Juana et al., 2010; Galán and Domínguez-Rodrigo, 2013).

In these studies, cut mark morphology analyses were restricted to optic microscopy, hand lenses and SEM (Shipman, 1981; Olsen, 1988; Greenfield, 1999, 2004, 2006a,b; Smith and Brickley, 2004; Lewis, 2008), binocular microscope for high resolution pictures (Domínguez-Rodrigo et al., 2009; De Juana et al., 2010; Marín-Monfort et al., 2014), digital imaging techniques (Gilbert and Richards, 2000), three-dimensional reconstruction

* Corresponding author.
E-mail addresses: mategonzalez@usal.es (M.Á. Maté González), joyravedra@hotmail.com (J. Yravedra), daguilera@usal.es (D. González-Aguilera).

http://dx.doi.org/10.1016/j.jas.2015.08.006
0305-4403/

(Bartelink et al., 2001; During and Nilsson, 1991; Kaiser and Katterwe, 2001), 3D digital microscope (Boschin and Crezzini, 2012; Crezzini et al., 2014), and a recent technique based on the use of Alicona 3D Infinite Focus Imaging microscope (Bello and Soligo, 2008; Bello et al., 2009; Bello, 2011; Bonney H., 2014).

These techniques basically recorded the main features of cut mark morphology (i.e. V-section of cut mark grooves) including variable length, width and depth depending on tool type, its raw material and bone morphology, inasmuch as the presence of internal microstriations which may be associated with secondary features such as barbs, shoulder effects or Hertzian cones (e.g. Martin, 1909; Binford, 1981; Shipman, 1981; Shipman and Rose, 1983). Although in most cases cut marks were described following two-dimensional observations, Bello and co-authors have used Alicona to interpret cannibalistic and funerary practices (Bello and Soligo, 2008; Bello et al., 2011a, 2015; Schulting et al., 2015), as well as to study teeth and the use of the mouth as a third hand (Hillson et al., 2010 Bello et al., 2011b). They also applied this method to the interpretation of engraved bones and antlers (Bello et al., 2013a) and the use of these materials as retouch tools and hammers (Abrams et al., 2014; Bello et al., 2013b). Boschin and Crezzini (2012) exemplified their technique in the analysis of archaeological collections to distinguish cut-marks produced by metal from stone-tool damage. The application of 3D technology was also used for engraved pottery (Montani et al., 2012) and prehistoric art (Güth, 2012).

The present article describes a methodology which overcomes the limitations implied in the use of microscopes -i.e. restricted

Table 1
Technical specifications, usage and classification of the tools used.

Tool	Classification	Working	Technical specifications
Trinocular stereoscopic microscope with image sensor.	Passive sensor	An image sensor is installed in the third observation channel of the microscopy and its optical is used as the objective.	• Euromex NOVEX AR Trino (Continuous Zoom 1X a 4X) + Reflex Camera Nikon D5100 (sensor CMOS de 23.6 × 15.6 mm de 16.2 MP) + Camera Adapter T-System. • Motic DM-39C–N9GO A (Fixed Zoom 2X a 4X) with digital camera included (CMOS 1/2″ 3 MP, Pixel matrix 2048 × 1536). • Motic SMZ-143 (Continuous Zoom 1X a 4X) + Reflex Camera Nikon D5100 (sensor CMOS of 23.6 × 15.6 mm of 16.2 MP) + Camera Adapter T-System.
Microscopic multifocal motorized with high-resolution digital camera included	Passive sensor	It corrects the limited field depth of macro-photography when the focal length, focus distance and diaphragm opening are reduced. The user has to focus the furthest and the nearest point of the object. The microscopic function takes those points as a reference and automatically makes a sequence of intermediate images of the same scene, changing the focus point. Finally, it joins those images and generates a single clear photography with each element focused in a precise way.	• Leica M 205C (Continuous Zoom 0.7X a 160X) + Sensor DFC 450 (CCD – ICX282 8.7 × 6.5 mm, 5 MP).
Digital portable microscopic USB	Passive sensor	The images obtained are only visible by computer software. A photograph collection is needed.	• Digital portable microscopic USB Celestron (Continuous Zoom 1X a 4X y 15x fixed). Digital camera (CMOS 1.3 MP, Pixel matrix 1280 × 1024).
Reflex camera + Reverse mounting adapter of objective	Passive sensor	The reverse mounting adapter of objective is an accessory placed between the body of the camera and the objective, which is placed in a reverse position. It simulates a macro objective.	• Reflex camera Nikon D5100 (sensor CMOS of 23.6 × 15.6 mm of 16.2 MP, pixel size of 4.78 μm) + Objective 18–55 mm + Reverse mounting adapter of objective of 52 mm.
Reflex camera + Extension Tubes of Objective	Passive sensor	The extension tubes of the objective are an accessory placed between the body of the camera and the objective, reducing the minimum lens focus distance. It simulates a macro objective.	• Reflex camera Nikon D5100 (sensor CMOS of 23.6 × 15.6 mm of 16.2 MP pixel size of 4.78 μm) + Objective 18–55 mm + Aluminium Extension Tubes of Objective of lengths 12 mm, 20 mm y 36 mm.
Reflex camera + Close-Up lens Macro Filter Set	Passive sensor	The close-up lens macro is a filter screwed at the end of the objective which increasing the image area, creating a loupe effect. It simulates a macro objective.	• Reflex camera Nikon D5100 (sensor CMOS de 23.6 × 15.6 mm of 16.2 MP pixel size of 4.78 μm) + Objective 18–55 mm + 52 mm Close-Up lens Macro Filter Set of 1X, 2X, 4X and 10X.
Reflex camera + Macro Objective	Passive sensor	Sensor system of images invented to focus at short distances, enlarging the elements focused three to four times. The result is high quality photographs.	• Reflex camera Canon EOS 50D (Sensor CMOS (APS-C) of 22.3 × 14.9 mm of 15.1 MP, pixel size of 4.7 μm) + Objective SIGMA 50 mm 1 2.8 dg macro
Metrological Laser Scanner	Active sensor	Metric recorder of an object with coordinates. As result, a 3D model is obtained.	• Hexagon Metrology Absolute Arm 7325SI. Measuring Range 2.5 m. Probing Point Repeatability ±0.079 mm. Probing Volumetric Accuracy ±0.069 mm. Scanning System Accuracy ±0.042 mm. Max. Point acquisition rate: 50.000 Points/s. Line Rate: 30 Hz. Accuracy (2 sigma): 30 μm).
Structured Light 3D Scanner	Active sensor	System made up of a camera, a projector and a calibration board. It must be first calibrated placing the camera and the projector in 15° and 25° angles towards the calibration board. The projection must cover the calibration board completely. The scale of the calibration board is specified in the software, the exposition of the camera is adjusted and the focus of the camera and the projector are verified in the tools. It needs to be calibrated as well. The camera and the projector must be fixed. The object substitutes the calibration board. The pictured is scanned and a 3D points cloud or a 3D model of the object is made.	• David Structured Light Scanner SLS-2. Scan size: 60 –500 mm. Resolution: Up to 0, 1% of scan size (down to 0.06 mm). Scanning time: One single scan within a few seconds. Mesh density: Up to 1,2000,000 vertices per scan = ACER K132 + Structured Light Projector + DAVID USB CMOS Monochrome Camera with Lens + DAVID Structured-Light Calibration Panels Set.

Table 2
Advantages and disadvantages of the different tools and techniques and if the method is appropriate or not.

Tools	Description of the technique	Advantages	Disadvantages	Conclusion
Trinocular stereoscopic magnifier with sensor of images.	Production of macro photography to use macro-photogrammetric techniques with vertical photograph captures.	+ The photographic sensor uses the microscopy optical as objective, taking detail photographs.	+ Very poor photograph quality if the object has relief. Due to the limited field depth, the photography looks badly focused. + It is not possible to take convergent photographs; they can only be perpendicular to the object. + It is a static tool: the object should be moved (not practical for photogrammetry). + Short distance between the object and the tool to make a right 3D reconstruction. + Static, heavy and difficult to use tool. + In some cases, bad illumination of the object. + Data collection and processing protocols are slow.	+ Perpendicular photograph capture at short distance does not generate quality geometric models. + Unfocused photograph of objects with relief. + The 3D models obtained do not have relief, they are flat. NO APPROPRIATE TECHNIQUE
Microscopic multifocal motorized with high-resolution digital camera included	Production of macro photography to use macro-photogrammetric techniques with vertical photograph captures.	+ Specific tool to make high detail and quality photographs of flat objects and elements with relief due to the internal system which creates a focused photograph from different joined images.	+ It is not possible to take convergent photographs; only pictures perpendicular to the object are taken. + It is a static tool: the object should be moved (not practical for photogrammetry). + Short distances between object and tool to make a good 3D reconstruction. + The pixels of the photograph generated by the microscopy are modified due to the matching images. + Static, heavy and difficult to use tool. + Data collection and processing protocols are slow.	+ Perpendicular photograph capture at short distance does not generate quality geometric models. + In the areas where the photography has a bigger alteration of pixels, the reconstruction of 3D models shows deformations. + The 3D models obtained do not have relief, they are flat. NO APPROPRIATE TECHNIQUE
Digital portable microscopic USB	Production of macro photography to use macro-photogrammetric techniques with vertical and convergent photograph captures.	+ High detail photographs can be made. + It is possible to see the microscopic image directly on the computer screen. + Effective.	+ Very low photographic quality, bad focus due to the little depth of field. + Short distance between the object and the tool to make a right 3D reconstruction. + Data collection and processing protocols are slow.	+ Digital images do not have enough quality. + Very distorted models, with no quality. NO APPROPRIATE TECHNIQUE
Reflex camera + Reverse mounting adapter of objective	Production of macro photography to use macro-photogrammetric techniques with vertical and convergent photograph captures.	+ Low cost macro photograph. + Good quality of image.	+ For convergent photography, the focus is bad in the extreme cases. + For perpendicular photography, the distance between the object and the tool is still small to get a good 3D reconstruction. + Data collection and processing protocols are slow.	+ In the cases of parallel photographs, the short distance capture of the object cannot generate good quality geometric models. + In the case of convergent photography, the photography capture with the biggest perspective has a focus problem. + The 3D models obtained do not have relief, they are flat. NO APPROPRIATE TECHNIQUE
Reflex camera + Extension Tubes for the Objective	Production of macro photography to use macro-photogrammetric techniques with vertical and convergent photograph captures.	+ Low cost macro photograph.	+ Poor photographic quality. + When the objective is opened out, little light is available, so better lighting is necessary. + For convergent photographs, the focus is not appropriated for the extremes. + For perpendicular photographs to the base line, the distance between the object and the tool is still small to get a good 3D reconstruction. + Data collection and processing protocols are slow.	+ Digital images of objects with relief do not have enough quality due to limited focus. + In the cases of parallel photographs, the short distance capture of the object cannot generate good quality geometric models. + In the case of convergent photography, the photography capture with the biggest perspective has a focus problem. + The 3D models obtained from vertical photography do not have relief, they are flat. + The 3D models obtained from the convergent photographs become distorted. NO APPROPRIATE TECHNIQUE
		+ Low cost macro photograph.		

Reflex camera + Close-Up lens Macro Filter Set	Production of macro photography to use macro-photogrammetric techniques with vertical and convergent photograph captures.		+ Increased objective optical distortion, more anomalies. + Poor photographic quality. + For convergent photograph, the focus is unsuitable for the extremes. + For perpendicular photographs to the base line, the distance between the object and the tool is still small to get a good 3D reconstruction. + Data collection and processing protocols are slow.	+ Digital images of objects with relief do not have enough quality due to limited focus. + In the cases of parallel photographs, the capture at a short distance to the object cannot generate good quality geometric models. + In the case of convergent photographs, the collection at a large perspective has a focus problem. + The 3D models obtained from vertical photographs do not have relief, they are flat. + The 3D models obtained from the convergent photographs become distorted. NO APPROPRIATE TECHNIQUE
Reflex camera + Macro Objective	Production of macro photograph to use macro-photogrammetric techniques with vertical and convergent photograph captures.	+ Good quality of image. + For convergent photograph, the focus is good in the extremes.	+ For perpendicular photographs, the distance between the object and the tool improves considerably but it is still not sufficient to get a good 3D reconstruction.	+ In the cases of parallel photographs, the capture at a short distance to the object cannot generate good quality geometric models. + The 3D models produced from vertical photographs do not have relief, they are flat. NO APPROPRIATE TECHNIQUE + Convergent photography: high quality 3D models. APPROPRIATE TECHNIQUE
Metrological Laser Scanner	Production of high-resolution 3D models for the use of computational vision techniques.	+ Fast data collection protocol. It is possible to scan many pieces in a short time. + The scanning provides a metric model to scale.	+ Poor scan resolution.	+ The metrological laser scanner does not have enough resolution to capture cut marks. NO APPROPRIATE TECHNIQUE
Structured Light 3D Scanner	Production of high-resolution 3D models for the use of computational vision techniques.	+ Once the system is configured, the data collection protocol is fast. It is possible to scan many pieces in a short time. + The scanning provides a metric model to scale. + Low cost system.	+ It is difficult to get good results. Significant differences between outputs.	+ Difficult to find an effective protocol for data collection, which allows obtaining always a good result without variations among different captures. NO APPROPRIATE TECHNIQUE

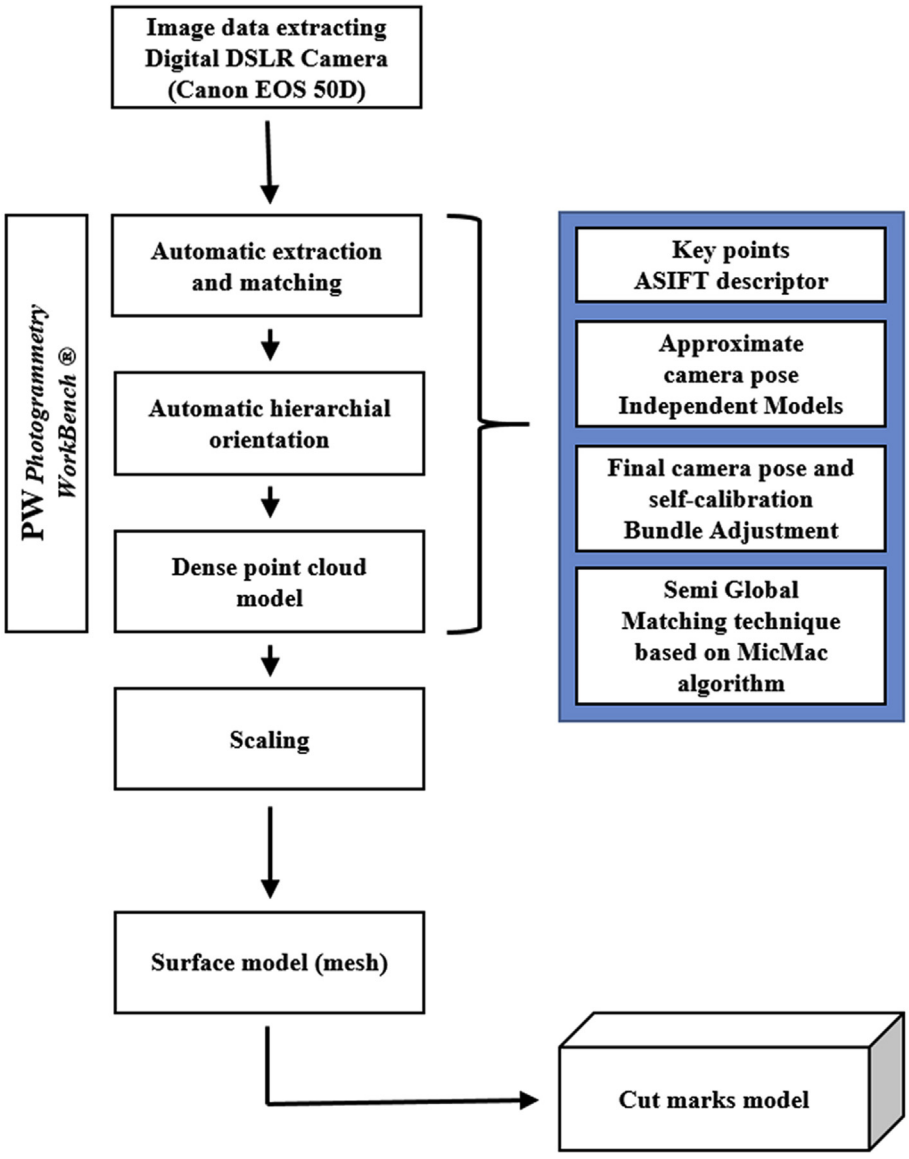

Fig. 1. Macro-photogrammetric protocol to generate the 3D model of cut marks.

access due to high costs-by reducing analytical costs and, consequently, enlarging the sample to be tested. This technique incorporates treatment of high-resolution images with macro-photogrammetry and computer visualisation for tri-dimensional reconstruction of cut marks on bones. These micromorphological data are later analysed in both qualitative and quantitative terms.

2. Materials and methods

In this study, different criteria were used (Table 1) for a morphometrical characterisation of cut marks on bones. A total of 15 cut marks made with a stainless steel knife (Molybdenum Vanadium C 0.5 CR 14 MO 0.5 VA 0.25) on three long bone diaphysis and a lamb scapula were examined with macro-photogrammetric and computer vision techniques which included different tools of microscopic and laser technology (Table 1). A single right-handed person performed all the marks on lamb fresh bones. The bones were later cleaned by boiling in tap water for the analyses.

The preliminary analysis showed that macro-photogrammetric techniques using photographs taken with a reflex camera with a macro function provided a better resolution than alternative approaches. Table 2 presents the advantages and disadvantages for each of the techniques used.

2.1. Macro-photogrammetric technique

A three-dimensional model of quantitative and qualitative information about the cut mark was drawn from a series of images and following an easy application protocol (see subsection 2.1.1.). Some of the most critical steps in the process were the orientation of the images regarding their angular and spatial positions, and the determination of the internal parameters of the camera (self-calibration). Fig. 1 illustrates the different steps involved in the macro-photogrammetric and computational vision method used for 3D modelling of images.

2.1.1. Image capture protocol

The methodology for macro-photogrammetric analysis required placing a millimetre scale next to the cut mark to be photographed so as to provide a precise measurement reference (Fig. 2).

Specimens were individually placed on a photographic table with lighting adjusted to keep the bone permanently well illuminated. The photographic sensor had to be configured at the beginning of the process to adjust focus and brightness. Several tests of different exposition and opening of the diaphragm were needed to verify the optimal parameters, as well as to calculate the distance needed for a good definition of the cut mark. Both the exposition moment of the camera and lighting remained constant during the image data capture.

For the capture of images, two kinds of configurations were followed: the parallel photography method (Fig. 3a) and the oblique and convergent photography method (Fig. 3b). The distance between the camera and the object was approximately 100–120 mm.

Parallel photography was composed of images captured at a perpendicular axis regarding the object photographed. Each picture was parallel, creating coplanar plans to the object with a minimum overlapping of 80% (Fig. 3a). Convergent photography, on the other hand, required taking photographs which converge in a point and do not need to be parallel (Fig. 3b). In this case, overlapping of photographs must be complete (100%). Furthermore, the two adjacent camera stations had to be generally placed at an intersection angle of about 15° to the object.

Both configurations presented certain advantages and disadvantages. The main advantage of parallel photogrammetry was to avoid the perspective becoming distorted. On the other hand, ray intersection geometry was rather poor, but it was especially important to have a good parameter when reconstructing depth and relief. Convergent photogrammetry offered a better ray intersection geometry, although the perspective became somewhat distorted, affecting the automatic reconstruction process.

The number of photographs for each model depended on the size and features of the relevant cut marks on the bone, as well as its position on either a flat or a bended plane.

Once the photographs had been taken, they were processed so as to generate a 3D model for each mark. Consequently, the photographs were treated with a photogrammetric reconstruction software such PW (Photogrammetry Workbench) (González-Aguilera et al., 2013) or another reconstruction software such Agisoft photoscan. PW software followed the workflow presented in Fig. 1.

2.1.2. Hierarchical orientation of images and self-calibration

The automatic orientation of the angular and spatial position of the images required the previous drawing and matching of certain features (i.e. points of interest). In particular, a variation in the algorithm SIFT (Scale-Invariant Feature Transform) (Lowe, 1999) called ASIFT (Affine Scale Invariant Transform) (Morel and Yu, 2009) had to be added, to improve the data collection by, for instance, considering two additional affinity parameters for perspective control (i.e. the two perspective angles of the optical axis of the camera, φ (tilt) angle and ϖ (axis) angle (Equation (1))). Therefore, the ASIFT algorithm was useful for the manipulation of images in perspective, frequent in these cases. The result was a keypoint algorithm, which presented no variation regardless of scale, rotation, movement, or main deformations caused by the different perspectives of the images. The following expression summarises the resulting affine scale invariant transformation:

$$\boldsymbol{A} = \begin{bmatrix} \boldsymbol{a} & \boldsymbol{b} \\ \boldsymbol{c} & \boldsymbol{d} \end{bmatrix} = H_\lambda R_1(\kappa) T_1 R_2(\varpi) = \lambda \begin{bmatrix} \cos\kappa & -\sin\kappa \\ \sin\kappa & \cos\kappa \end{bmatrix} \cdot \begin{bmatrix} t & 0 \\ 0 & 1 \end{bmatrix} \cdot \begin{bmatrix} \cos\varpi & -\sin\varpi \\ \sin\varpi & \cos\varpi \end{bmatrix} \quad (1)$$

where **A** was the affine transformation with the λ scale, and κ the rotation of the optical axis (swing). The perspective parameters for the inclination of the optical axis of the camera were represented by φ (tilt) = across $(1/t)$, the angle between the optical axis and the normal of the image plane and ϖ (axis), the azimuth angle between the optical axis and a fixed vertical plane.

Taking into account the data generated by ASIFT, the image was oriented following a double procedure involving computer vision and photogrammetry to reach an approximate orientation of the images in an arbitrary coordinates system (computer vision) which could be later refined and improved to assemble the images (photogrammetry).

It was necessary to relatively orientate the images by using independent models, as well as calculating the fundamental matrix using the Longuet–Higgins algorithm (Longuet-Higgins, 1987). One of the main advantages of the fundamental matrix was its independence from the scene pictured. Therefore, the matrix could be calculated from the corresponding point in the image, regardless the internal parameters and original approximations of the cameras. The fundamental matrix was defined by the following Equation (2):

$$\boldsymbol{x}'^{T}\mathbf{F}\boldsymbol{x} = 0 \quad (2)$$

For each pair of matching points $x_i \leftrightarrow x'_i$ (8 minimum), Equation (3) calculated the fundamental matrix. More specifically, by writing $x = (x,y,1)$ and $x' = (x',y',1)^T$, each matching point created a linear equation,

$$x'xf_{11} + x'yf_{12} + x'f_{13} + y'xf_{21} + y'yf_{22} + y'f_{23} + xf_{31} + yf_{32} + f_{33} = 0 \quad (3)$$

It should be noted that this procedure was completely automatic compared with other photogrammetric approaches where the user needed to set the initial approximations and know the internal parameters of the camera. Secondly, once the relative angular and spatial position of the images were established, a comprehensive bundle adjustment was made by an iterative and least-squares process based on the co-linearity condition (Kraus, 1993) and adding the object coordinates for fully georeferencing the images (Equation (4)). Object coordinates were incorporated into the

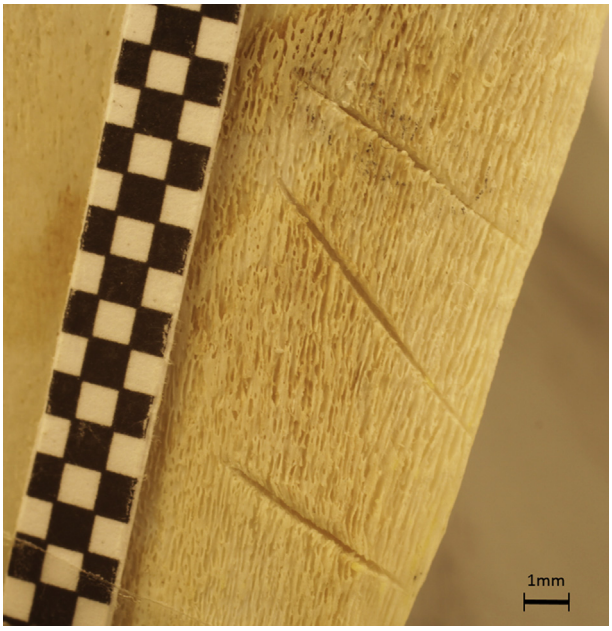

Fig. 2. Photography of cut marks. The millimetre reticule can be seen next to the marks.

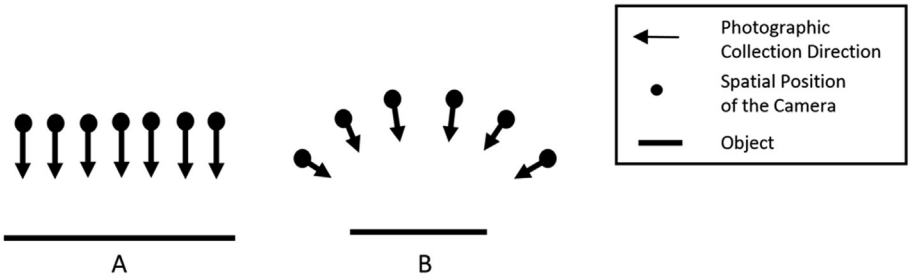

Fig. 3. (a) Parallel photography capture. (b) Oblique and convergent photography capture.

orientation process from the millimetre reticule placed on the object (Fig. 2). When the internal calibration parameters (i.e. focal length, principal point and lens distortion) were unknown, this step adds to the equation the camera calibration parameters as unknown quantities (self-calibration).

$$(x - x_0) + \Delta x = -f\frac{r_{11}(X - S_X) + r_{21}(Y - S_Y) + r_{31}(Z - S_Z)}{r_{13}(X - S_X) + r_{23}(Y - S_Y) + r_{33}(Z - S_Z)}$$
$$(y - y_0) + \Delta y = -f\frac{r_{12}(X - S_X) + r_{22}(Y - S_Y) + r_{32}(Z - S_Z)}{r_{13}(X - S_X) + r_{23}(Y - S_Y) + r_{33}(Z - S_Z)} \quad (4)$$

where x and y were the image coordinates; X, Y, Z were the object control points coordinates, corresponding to the millimetre reticule placed on the object which placed the scale in the scene; r_{ij} were the rotation matrix elements, including the rotation of the camera; S_X, S_Y, S_Z were the object coordinates of the camera viewpoints; f was the main distance; x_0, y_0, the main point coordinates of the image; and ΔX, ΔY represented the translations due to the radial and tangential distortion of the lens. In case these internal parameters of the camera were unknown, they were thus indicated (self-calibration) in the calculation of the global adjustment.

2.1.3. Dense model generation

The dense matching process started with the robust image orientation, based on the semi-global matching technique (SGM) (Hirschmuller, 2005; Deseilligny and Clery, 2011). The projective Equation (5) generated a dense model from the identification of a 3D coordinate per pixel.

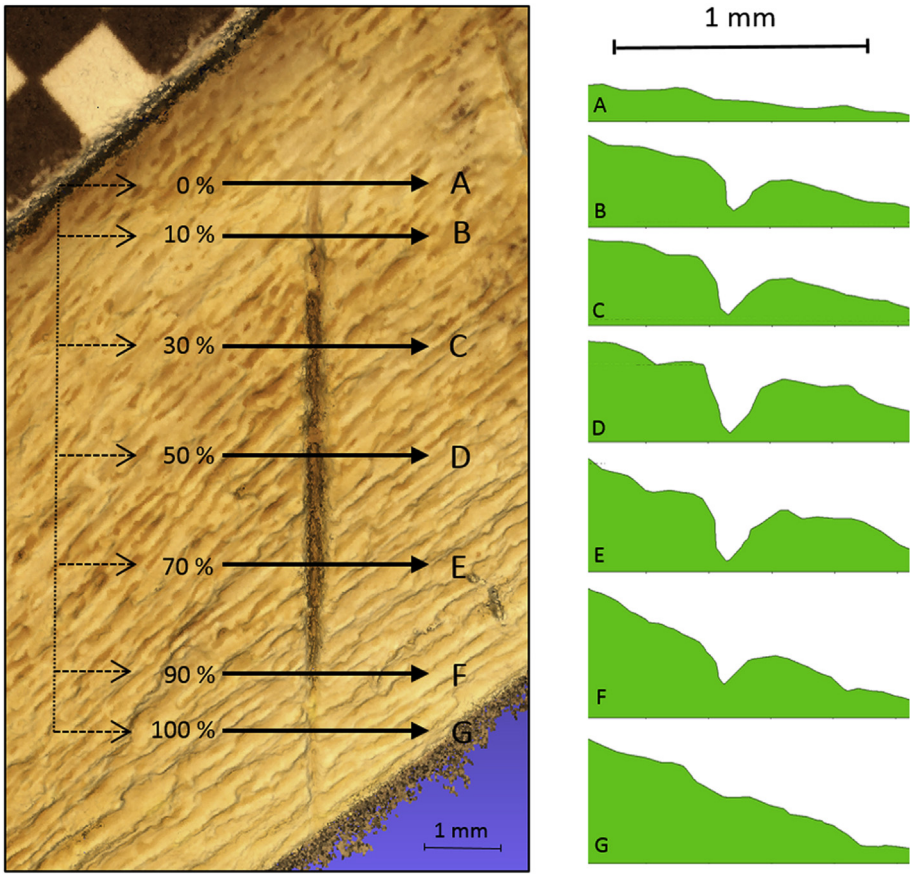

Fig. 4. Cut marks analysis: cross sections from different relative positions along the cut mark.

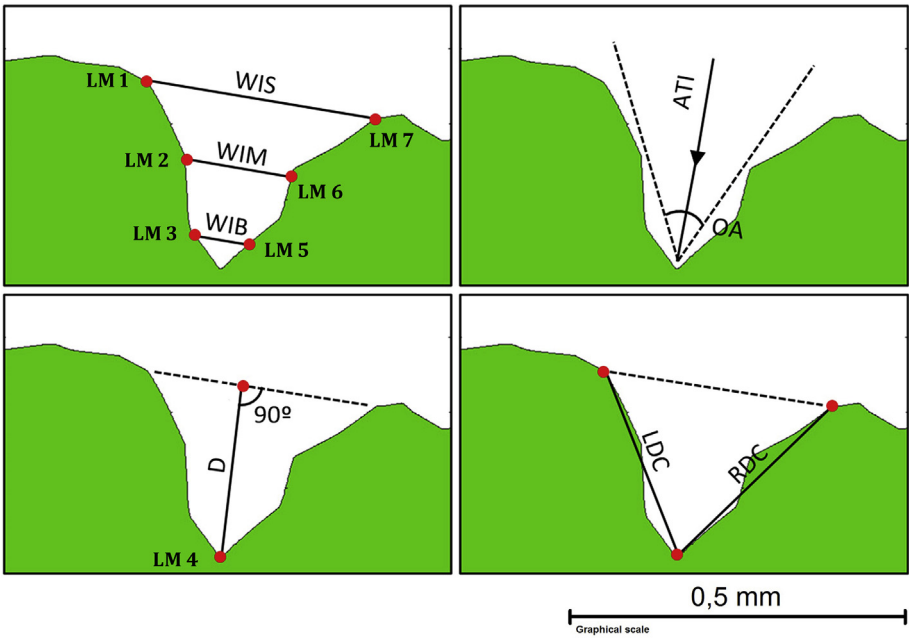

Fig. 5. Representation of the measures for each mark cross-profile (following Table 3), and the location for the 7 landmarks used in the morphometric analysis (LM 1–7).

$$x_k = C(D(R_i(X_k - S_i))) \tag{5}$$

Where X was the 3D point; x was the point corresponding to the image; R was the camera rotation matrix; S was the camera projection centre; C was the internal calibration function; D was the lens distortion function, and the subscripts k and i were related to point and image, respectively.

The SGM process consisted of minimising an energy function (6) through the eight basic directions a pixel could follow (every 45°). This function was integrated by a cost function (i.e. M, pixel matching cost), which reflected the similarity of the pixels in two images (x and x'), together with the incorporation of two restrictions, P_1 and P_2, which showed the possible presence of outliers in the SGM process. In addition, a third constraint was added to the SGM process: epipolar geometry, derived from photogrammetry (Hartley and Zisserman, 2003). It restricted the search space per pixel in order to reduce the huge computational cost involved. As a result, it generated a dense model with multiple images, obtaining optimal processing times.

$$E(D) = \sum_x \left(M(x, D_x) + \sum_{x' \in N_x} P_1 T[|D_x - D_{x'}| = 1] + \sum_{x' \in N_x} P_2 T[|D_x - D_{x'}| > 1] \right) \tag{6}$$

Table 3
Measurements used to characterize the cut mark sections as described in Fig. 5.

WIS	Width of the incision at the surface
WIM	Width of the incision at the mean
WIB	Width of the incision at its bottom
OA	Opening angle of the incision
D	Depth of the incision
LDC	Left depth of the incision convergent
RDC	Right depth of the incision convergent
ATI	Angle of the tool impact

Where $E(D)$ was the energy function to be minimised on the basis of the disparity (parallax) between homologous features; the function C (pixel matching cost) evaluated the level of similarity between the pixel p and its counterpart q through the disparity D_p, while P_1 and P_2 corresponded to two restrictions aimed to avoid outliers in the dense matching process due to the disparity of one single pixel or many of them respectively.

2.2. Cut mark analysis

The completion of 3D models of cut marks was followed by a thorough analysis of the morphology and section of the traces. The 3D model allowed an infinite number of sections to be defined along the groove. This method, however, offered an objective selection of sections to compare among different marks. Each cut mark was divided into equidistant sections, comprising the 0% (A), 10% (B), 30% (C), 50% (D), 70% (E), 90% (F) and 100% (G) of the mark length (Fig. 4). Sections corresponding to B, C, D, E and F were subsequently measured. The first and last sections (A and G) were not included as they represented the beginning and end of a mark.

Measurements were expressed as independent variables, following Bello et al. (2013a) (Fig. 5). These measurements indicated the thickness, depth, and angles of the mark (see Table 3).

2.3. Statistical analysis

In order to test if there was any difference in the several measurements, a variance analysis (ANOVA) was applied. However, this analysis required previously the use of Bartlett's test in order to confirm that variance was homogeneous throughout the sample. Those values indicating significant variation among section types were thus subjected to multiple variance analysis (MANOVA) for the comparison of metric variables and the determination of the mean values for the five-section grouping proposed.

As an independent confirmation method, a principal component analysis (PCA) was also performed to study the overlapping of the five subsamples (as per mark section) beyond their differences in

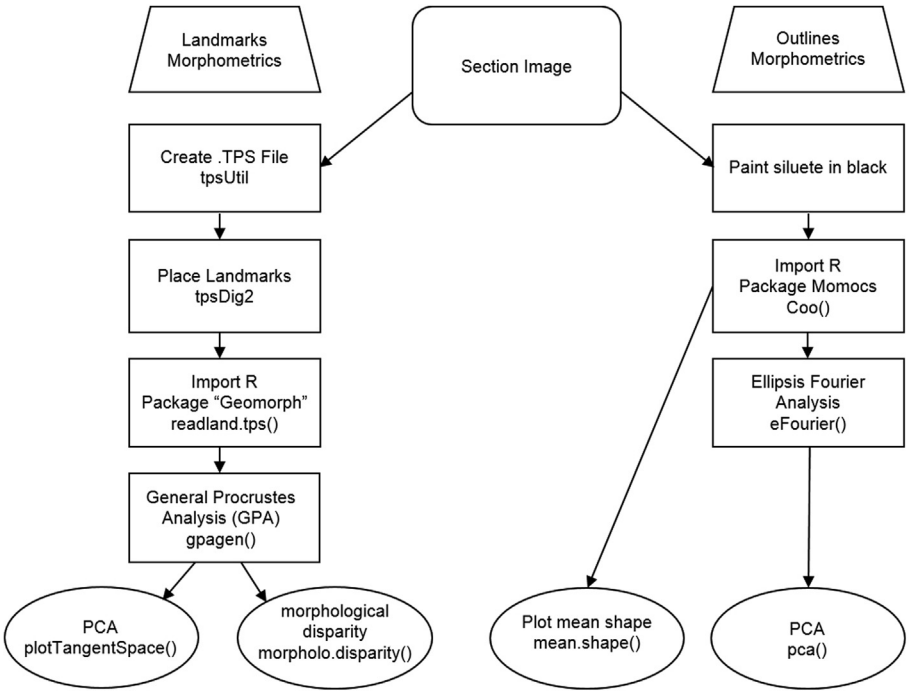

Fig. 6. Diagram of the morphometric analysis used in this research.

Table 4
Main technical data from the 3D models created. GSD (9) (Ground Sample Distance) is the equivalence of the image pixel on the ground, D is the distance to the object, F is the focal length and pixel size p.

	Fieldwork						
	Measurements cut marks (mm)				N° of images	Distance max/min (m)	Fieldwork (minutes)
	Cut mark	Length	Width	Height			
Model 1	1	7.221	0.297	0.222	7	0.12/0.1	12
Model 2	2	3.952	0.321	0.205	6	0.12/0.1	12
Model 3	3	5.229	0.418	0.142	13	0.12/0.1	12
	4	4.994	0.419	0.191			
Model 4	5	3.577	0.245	0.136	5	0.12/0.1	12
Model 5	6	3.811	0.261	0.216	5	0.12/0.1	12
Model 6	7	3.353	0.635	0.295	11	0.12/0.1	12
Model 7	8	2.377	0.645	0.233	9	0.12/0.1	12
Model 8	9	3.471	0.652	0.109	11	0.12/0.1	12
	10	3.214	0.624	0.142			
Model 9	11	7.251	0.673	0.255	9	0.12/0.1	12
Model 10	12	6.082	0.308	0.156	9	0.12/0.1	12
Model 11	13	2.267	0.53	0.221	9	0.12/0.1	12
Model 12	14	2.265	0.447	0.11	10	0.12/0.1	12
Model 13	15	3.757	0.304	0.178	5	0.12/0.1	12

	Laboratory work							
	Tie points	N° matching points	GSD (mm)	Photogrammetric adjustment error (mm)	Scaling error (mm)	Total error (mm)	Resolution (mm/pixel)	Laboratory work (minutes)
Model 1	24,928	2,772,921	0.0103	±0.0076	±0.0166	±0.0183	±0.0094	35
Model 2	16,603	7,771,843	0.0103	±0.0086	±0.0166	±0.0187	±0.0047	30
Model 3	43,622	4,255,532	0.0103	±0.0089	±0.0166	±0.0188	±0.0093	65
Model 4	12,459	2,273,766	0.0103	±0.0088	±0.0166	±0.0188	±0.0096	35
Model 5	4592	2,101,687	0.0103	±0.0183	±0.0166	±0.0247	±0.0095	35
Model 6	1515	3,127,808	0.0103	±0.0198	±0.0166	±0.0258	±0.0217	60
Model 7	1683	3,062,299	0.0103	±0.0192	±0.0166	±0.0254	±0.0204	40
Model 8	1941	3,317,796	0.0103	±0.0166	±0.0166	±0.0235	±0.0221	60
Model 9	1468	3,289,203	0.0103	±0.0142	±0.0166	±0.0218	±0.0201	40
Model 10	1682	3,707,530	0.0103	±0.0178	±0.0166	±0.0243	±0.0093	40
Model 11	1955	2,773,400	0.0103	±0.0616	±0.0166	±0.0231	±0.0234	40
Model 12	1904	2,555,692	0.0103	±0.017	±0.0166	±0.0237	±0.0242	45
Model 13	5523	1,857,879	0.0103	±0.0128	±0.0166	±0.0209	±0.0095	35

$GSD = \frac{p \cdot D}{f}$ (9).

mean values per metric variables which resulted from the previous variance analysis. Biplots with 95% confidence ellipses were used.

ANOVA and MANOVA tests were performed with R (www.r-project.org) software (Core-Team, 2013). Furthermore, PCA is included in the R library FactoMineR (Lê et al., 2008). Plotting of the PCA results with confidence ellipses was made with the ggplot2 R library.

A geometric morphometric analysis was performed as well as a GPA as a supplementary alternative to the multivariate metric analysis (Fig. 6). Two morphometric approaches were used here: landmarks and outlines. Seven identical landmarks per section were considered from each mark using the tpsUtil (v. 1.60) and tpsDig2 (v. 2.1.7) programs. The location of the seven landmarks responded to the measures considered for the statistical analysis, as seen in Fig. 5. Thus, LandMark 1 (LM) was found at the beginning of the left line in the mark section. LM2, appeared in the middle of this line. LM3 was placed approximately at 10% of end of the mark. LM4 was at the very end, and LM5, LM6 and LM7, in an opposed position to LM3, LM2 and LM1, (Fig. 5). The resulting tps file was imported to R and analysed via the "geomorph" library (Sherratt, 2014).

A general Procrustes analysis (GPA) was later applied on the landmark data, followed by a PCA. Morphometric disparity analysis was possible by using the morphol.disparity function, which estimated the group distances via the diagonal sum of the covariance matrix (Zelditch et al., 2012).

The morphometric analysis of the outlines used the R library Momoocs. The mean shape per section was established (with the mean. shape function) and a Fourier Analysis was subsequently used to analyse outline shape similarities and differences.

3. Results

The definition of an appropriate optimum-resolution alternative method for cut marks analysis demanded a series of tools and techniques, as described in Table 1.

3.1. Results of the macro-photogrammetric method

As mentioned above, a large variety of analytical tools were reviewed in order to find a technique for generating high quality 3D models to be used in the geometrical study of cut marks on bones. Each of them followed some protocols and presented specific characteristics which determined their potential. Furthermore, the revision indicated that in most cases they did not seem suitable for this kind of analysis due to either data collection or post-processing time.

The macro-photogrammetric method, which was based on oblique photography and uses a reflex camera with macro lens, showed the best results in all study cases analysed, meeting the precision and short capture and post-processing time requirements. Particularly, an average time of 50 min was required to analyse a single cut-mark. Further details about the time required at field and laboratory work is described in Table 4. The accuracy for this method has already been demonstrated in other

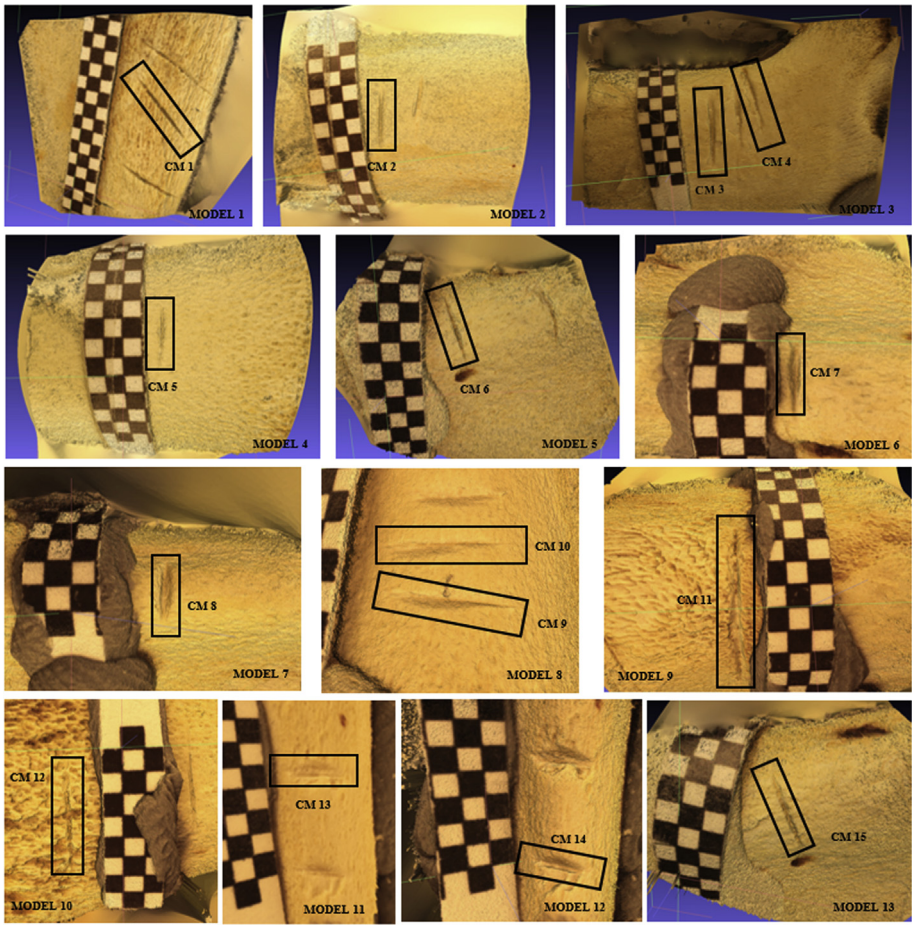

Fig. 7. 3D models of the different bones and cut marks analysed, where CM = Cut Mark.

Table 5
Measurement, distances (mm) and angles (°), from the sections of the different cut marks on bones, according to Bello et al., 2013a. See Fig. 5.

		WIS	WIM	WIB	OA	D	LDC	RDC	ATI
Mark 1	B	0.2481	0.1098	0.0393	61°	0.1492	0.1986	0.1889	76°
	C	0.324	0.1275	0.0472	63°	0.1862	0.2498	0.2439	79°
	D	0.3211	0.177	0.0471	56°	0.2484	0.2916	0.3	83°
	E	0.3129	0.1438	0.0479	54°	0.2311	0.2675	0.2918	79°
	F	0.279	0.1089	0.0333	64°	0.1434	0.1889	0.212	77°
Mark 2	B	0.3475	0.1948	0.0947	91°	0.1446	0.1999	0.2545	89°
	C	0.3147	0.2097	0.0514	74°	0.1804	0.1996	0.2883	84°
	D	0.3141	0.1728	0.0544	60°	0.233	0.2673	0.2964	84°
	E	0.3009	0.1726	0.038	64°	0.2018	0.2391	0.2656	86°
	F	0.328	0.2226	0.0559	91°	0.1456	0.234	0.2053	89°
Mark 3	B	0.3103	0.2162	0.0953	114°	0.0983	0.1703	0.1974	94°
	C	0.4004	0.2589	0.1037	109°	0.1154	0.3174	0.1559	104°
	D	0.4267	0.3008	0.1055	100°	0.148	0.3339	0.1953	99°
	E	0.5369	0.3502	0.136	111°	0.1639	0.3896	0.2461	95°
	F	0.4139	0.2931	0.1141	108°	0.111	0.3383	0.1457	104°
Mark 4	B	0.4749	0.3023	0.1003	120°	0.0942	0.1308	0.3956	88°
	C	0.3936	0.2016	0.0345	77°	0.1813	0.2167	0.3292	85°
	D	0.3876	0.1854	0.0285	71°	0.212	0.2491	0.333	80°
	E	0.4286	0.227	0.1174	92°	0.1788	0.2524	0.3077	81°
	F	0.4106	0.2687	0.0404	102°	0.1576	0.2177	0.3044	77°
Mark 5	B	0.223	0.1493	0.0314	105°	0.0838	0.1525	0.1271	90°
	C	0.2476	0.1492	0.0329	91°	0.0995	0.2097	0.1168	93°
	D	0.2754	0.1633	0.0541	70°	0.1726	0.2402	0.2038	80°
	E	0.2393	0.107	0.027	74°	0.1351	0.2041	0.1603	89°
	F	0.241	0.1517	0.0323	109°	0.0787	0.1703	0.1196	80°
Mark 6	B	0.1091	0.0529	0.0105	48°	0.0911	0.0976	0.1174	96°
	C	0.3396	0.17	0.0587	63°	0.2089	0.3044	0.2401	100°
	D	0.3551	0.1563	0.0408	59°	0.2352	0.2905	0.299	95°
	E	0.3245	0.225	0.0355	69°	0.2032	0.311	0.2218	95°
	F	0.1748	0.1064	0.017	65°	0.1299	0.1644	0.1501	98°
Mark 7	B	0.3545	0.196	0.0497	122°	0.0849	0.1531	0.2424	91°
	C	0.552	0.3648	0.0757	90°	0.2567	0.3135	0.4519	84°
	D	0.6967	0.3452	0.0655	80°	0.3053	0.4389	0.4886	86°
	E	0.6553	0.353	0.0829	81°	0.3219	0.3857	0.5479	82°
	F	0.6292	0.3388	0.0653	102°	0.2272	0.3879	0.3883	86°
Mark 8	B	0.4103	0.2656	0.0639	125°	0.106	0.2146	0.2476	125°
	C	0.6859	0.4249	0.1421	105°	0.2486	0.4159	0.4313	129°
	D	0.6682	0.4121	0.1118	97°	0.261	0.345	0.5138	127°
	E	0.5809	0.3713	0.1321	107°	0.1893	0.2801	0.4196	130°
	F	0.5324	0.3149	0.1029	97°	0.1961	0.1961	0.4275	129°
Mark 9	B	0.1674	0.1091	0.0306	111°	0.0519	0.0811	0.1173	84°
	C	0.6806	0.3783	0.0485	147°	0.0998	0.3383	0.371	85°
	D	0.6356	0.3326	0.0902	136°	0.1146	0.3166	0.3592	84°
	E	0.6408	0.3403	0.0236	135°	0.1132	0.2726	0.4089	84°
	F	0.6424	0.3847	0.1697	130°	0.1103	0.242	0.4411	76°
Mark 10	B	0.3516	0.2191	0.0926	132°	0.0675	0.2522	0.1279	105°
	C	0.5541	0.3022	0.0943	130°	0.127	0.2891	0.3205	94°
	D	0.6814	0.3794	0.0593	128°	0.1549	0.3617	0.3869	95°
	E	0.6359	0.3444	0.0538	127°	0.1429	0.3102	0.3879	91°
	F	0.4812	0.2364	0.065	131°	0.093	0.2065	0.3111	86°
Mark 11	B	0.7498	0.3907	0.0895	104°	0.2391	0.4865	0.4043	104°
	C	0.6689	0.3197	0.0894	105°	0.2372	0.4622	0.3611	100°
	D	0.6094	0.3568	0.0662	95°	0.253	0.4072	0.3851	100°
	E	0.7392	0.3595	0.0868	93°	0.2759	0.5499	0.3815	101°
	F	0.6255	0.3859	0.0631	117°	0.1652	0.4256	0.2859	103°
Mark 12	B	0.3769	0.2229	0.0418	133°	0.0708	0.1484	0.2566	91°
	C	0.2912	0.1642	0.0275	83°	0.1408	0.2062	0.1987	102°
	D	0.3502	0.1784	0.0266	79°	0.1572	0.2112	0.2613	90°
	E	0.283	0.1894	0.0131	81°	0.1689	0.2041	0.2254	92°
	F	0.326	0.1932	0.042	129°	0.0707	0.2124	0.1445	96°
Mark 13	B	0.6149	0.2853	0.0478	83°	0.2286	0.3839	0.3823	99°
	C	0.4792	0.2814	0.0655	83°	0.2109	0.3853	0.2628	99°
	D	0.5129	0.2873	0.0675	73°	0.2401	0.3652	0.3379	108°
	E	0.599	0.3399	0.1411	95°	0.2118	0.476	0.2732	97°
	F	0.3021	0.1504	0.0439	120°	0.0755	0.2116	0.129	81°
Mark 14	B	0.4627	0.2856	0.1435	94°	0.1018	0.1149	0.4219	85°
	C	0.5765	0.3941	0.1164	95°	0.1111	0.1153	0.5567	88°
	D	0.4038	0.2816	0.1153	90°	0.1202	0.1278	0.3775	87°
	E	0.362	0.2211	0.1356	99°	0.0973	0.0973	0.3306	83°
	F	0.3745	0.237	0.094	142°	0.0612	0.1658	0.228	89°
Mark 15	B	0.1695	0.132	0.0321	87°	0.0823	0.1074	0.0129	78°
	C	0.333	0.1681	0.0684	60°	0.2023	0.2335	0.3025	77°
	D	0.3808	0.1867	0.0536	70°	0.1969	0.2262	0.3337	82°
	E	0.3133	0.1583	0.0484	83°	0.1353	0.1911	0.2238	88°
	F	0.3209	0.146	0.0238	120°	0.0741	0.1437	0.2112	88°

micro-photogrammetric experiments (Rodriguez-Martin et al., 2015a, b).

Fig. 7 shows the 3D modelling of the 15 cut marks analysed, while Table 4 presents the technical data of the 3D models created. Regarding cut marks measurements, Table 5 explains the dimensional analysis according to the data in Fig. 5.

In order to estimate the total error (ε) associated to the dimensional analysis of cut marks using the macro 3D models generated, the error propagation had to be analysed by quadratic error propagation. Two main sources of errors were identified during the macro image-based modelling process proposed: first, the error coming from the photogrammetric adjustment, known as a posteriori error (ε_a); and second, the error corresponding to the scaling of the 3D model which was manually defined by the user. The latter was established as (7) $\sqrt{2}\times$ pixel size (s), considering the error associated to the electronic micrometre (destination error) ($\varepsilon_m = 0.01$) as well. Hence, the scaling error was calculated as:

$$\varepsilon_s = \sqrt{\varepsilon_m^2 + 2s^2} \tag{8}$$

More details about this error budget were outlined in Table 4.

As shown in the tables presented *supra*, some of the measurements of the cut mark sections (Table 5) were smaller than the total error of the models (Table 4). These measurements were only considered as estimates for the statistical analysis and did not imply any significant modification to the morphologic study of the cut mark.

The marks yielded a typical morphology with a V section, a straight groove and variable dimensions, with maximum lengths differing in each mark and ranging between 7.25 mm in mark 11, and 2.27 mm in marks 13 and 14. Mark width and depth were also variable (Table 5). The tool used in these experiments (metal knife) conditioned the absence of microstriations parallel to the principal axis of the mark (Figs. 2 and 4). However, given the variability of marks produced in this experiment, certain specifications were due regarding the differences and the possibility that some measurements of width, depth or other variables described in Fig. 5 were conditioned by the location (type of section) analysed. This was a key question as the results determined the most diagnostic sections to characterise cut mark dimensions and morphometry. Consequently, the most informative sections could be used to compare marks generated with raw materials or kinds of tools in the future.

The Bartlett test showed homogeneity of variance, which allowed the application of the ANOVA test (Fig. 8). This yielded significant differences in four variables, OA, D, LDC and RDC, which were selected for the MANOVA analysis. In turn, the MANOVA test confirmed the inter-section metric differences and allowed the recognition of inter-section differences via a pairwise comparison (Fig. 9). It showed that mark width, regardless the section chosen, was homogeneous; therefore the widths of WIS, WIM and WIB were similarly diagnostic of the mark morphology in each section. On the contrary, OA, D, LDC y RDC showed differences according to the section considered.

A PCA demonstrated that, despite the differences in mean values for the five sections, the overall confidence intervals of each section overlapped, making their identification extremely difficult. Only sections B and F had a differing tendency, probably due to greater

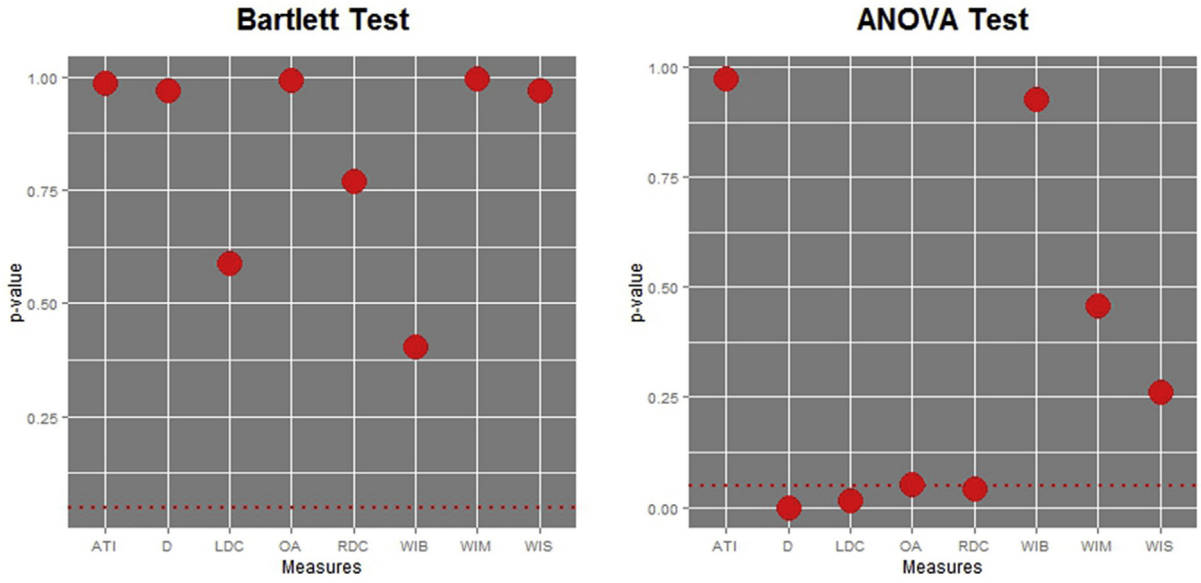

Fig. 8. Results of the Bartlett and ANOVA tests.

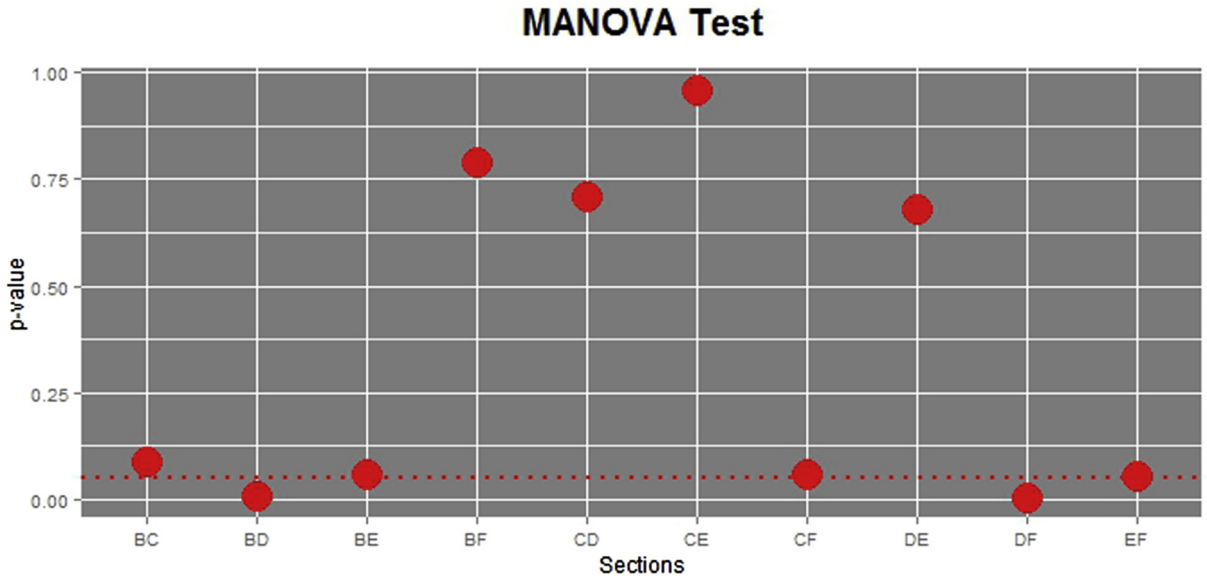

Fig. 9. Result of the MANOVA test.

variability at the beginning and end of the cut marks. The central sections yielded more homogeneous morphologies; therefore sections, C, D and E were the best ones to characterise the section morphology of the mark (Fig. 10).

The landmark geometric morphometric analysis reported an even more intense overlapping of section morphology, being virtually impossible to differentiate each of the five segments (Figs. 11 and 12). It was further confirmed by the morphological disparity analysis. None of the sections presented a significant p-value; it meant that no significant morphological differences were detected. Similar results were provided by the outline geometric morphometric analysis, as seen in the PCA graphics (Fig. 13).

Despite the seemingly variability reflected in the measurements of the different cut marks (Table 5), the tests performed indicated such small differences that they could hardly be considered significant (Figs. 11–13). This was especially true in the case of section width, variables WIS, WIM y WIB and the rest of the variables in sections C–E, which were slightly divergent from sections B and F. So, for a confident comparison of cut marks made with different raw materials or tool types, the values for the sections between 30% and 70% of the mark length would be the most representative one.

4. Conclusions

This article described the tools, methods and results from the geometric study of cut marks on bones by applying macro-photogrammetric and computer vision techniques. This proposal aimed to develop a low cost methodology precise enough to

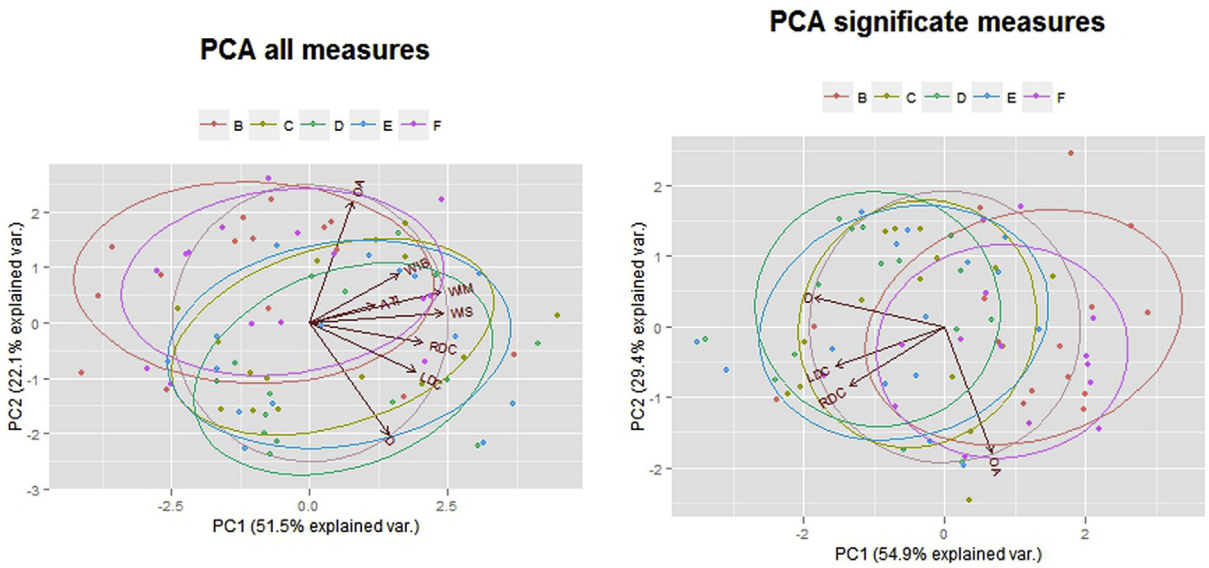

Fig. 10. PCA tests with all measures (left) and only representative measures (right).

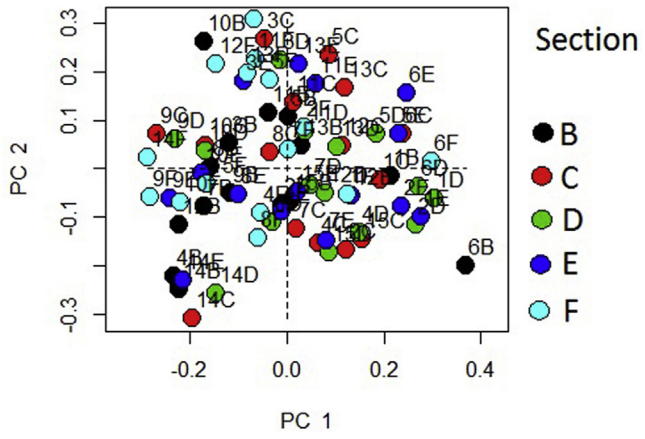

Fig. 11. PCA test of landmark-based morphometrics.

reproduce the results of more costly and difficult-to-access equipment, such as SEM, the new technical 3D digital microscope, or Alicona 3D Infinite Focus Imaging.

In order to define the methodology presented in this article, a wide range of techniques were tested (Table 2). Both methods used by laser techniques (structured lighting and optical triangulation) did not provide the needed resolution. Regarding fotogrametric techniques using parallel photography (Fig. 3a), 3D models looked flat and occationally deformed. The main reason for this problem when using a microscope was its mobility in the cenital axis rather than in the X and Y axes. It implied the need to move the object in those axes in order to photograph it. However, it was not recommended in photogrametry as the object should be kept still and the sensor would move. In the case of using a photographic camera supplemented by specific, the limited distance between the object and the sensor did not favor beams intersection in the 3D reconstruction and reduced the quality of the models. Finally,

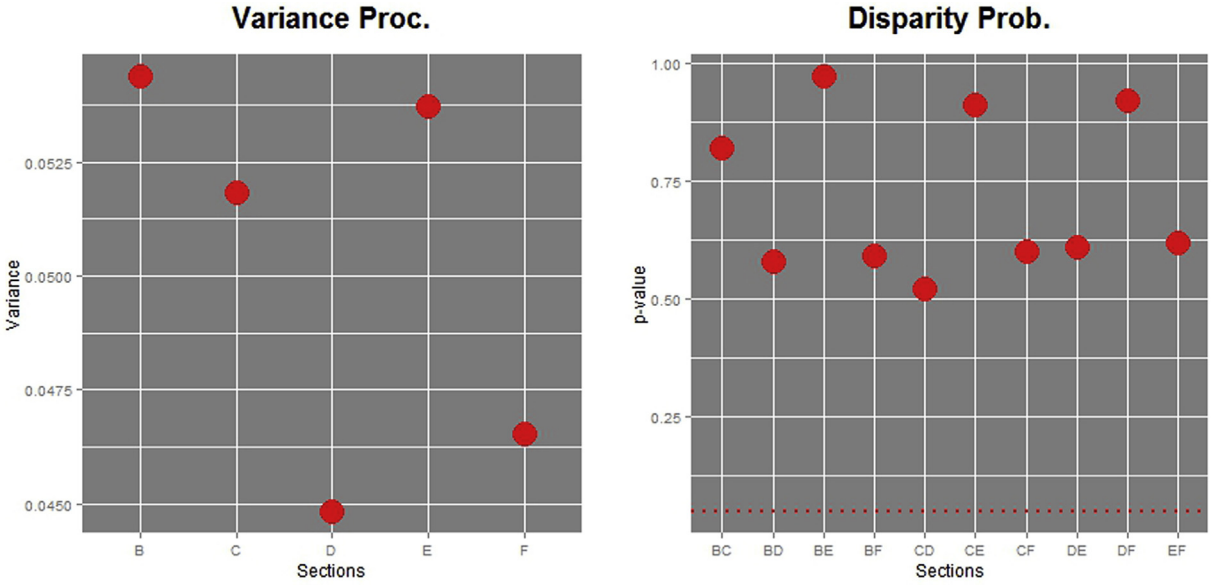

Fig. 12. Results of disparity tests.

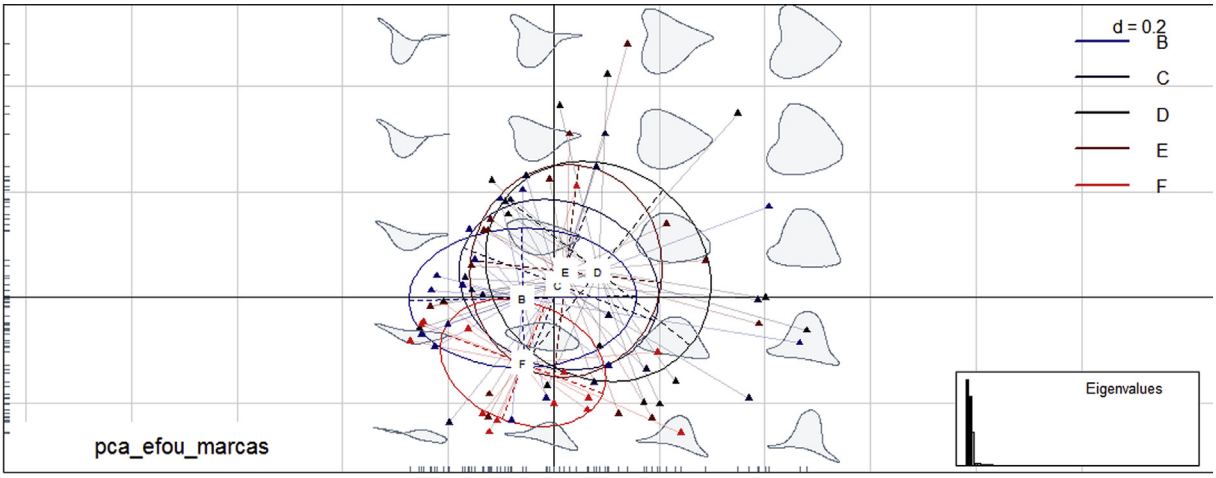

Fig. 13. PCA test of outlines morphometrics.

photogrametric techniques which used oblique photography (Fig. 3b) supplementing the camera with a specific gadget provided a more stable and better system to take the photographs, significantly improving the quality of the images. Hence, the method chosen includes a camera and an additional macro objective.

It may be concluded that it was possible to develop a fast and profitable method that generated high quality (average GSD (mm) = 0.0103; average precision (mm) = ±0.0221) 3D models of cut marks on bones. It was based on improved photogrammetry, together with computer vision techniques and the algorithms and numeric methods which transformed 2D (images) into 3D (point clouds) in an automatic, flexible and high-quality way. In this sense, macro-photogrammetric methodology was better than laser systems, generating higher quality and better resolution 3D models.

In this paper, an alternative method for the study of cut marks by using the in-house tool PW (Photogrammetry Workbench) was explained. The procedure described facilitated a more precise analysis of cut marks and the study of larger samples of bones with cut marks in a short time. The similarities between the values in most sections (30%–70% of the groove) further showed that the location to be studied may be equally efficient, enabling the morphological comparison of marks made with different tool types, raw materials or the age pattern of the different individuals in the future. The preliminary analyses in process seem to indicate differences between the cut marks produced with varying materials, such as the absence of microestriations in the cut marks produced with metal tools when compared to stone flakes.

Acknowledgements

The authors would like to thank the TIDOP Group from the Department of Cartographic and Land Engineering of the High Polytechnics School of Ávila, University of Salamanca, for the use of tools and facilities. We also want to thank Jesús de Vicente y Oliva, industrial engineer and teacher at the Polytechnics University of Madrid for his help. We also want to thank Aixa Vidal for the translation and revision of this paper. Finally, our gratitude to Yolanda Fernandez Jalvo for her comments on a previous draft and to the anonymous reviewers.

References

Abrams, G., Bello, S.M., Di Modica, K., Pirson, S., Bonjean, D., 2014. When Neanderthals used cave bear (Ursus spelaeus) remains: bone retouchers from unit 5 of Scladina Cave (Belgium). Quat. Int. 326–327, 274–287.

Bartelink, E.J., Wiersema, J.M., Demaree, R.S., 2001. Quantitative analysis of sharp-force trauma: an application of scanning electron microscopy in forensic anthropology. J. Forensic Sci. 46, 1288–1293.

Behrensmeyer, A.K., Gordon, K.D., Yanagi, G.T., 1986. Trampling as a cause of bone surface damage and pseudo-cutmarks. Nature 319, 768–771.

Bello, S.M., 2011. New results from the examination of Cut-Marks using three-dimensional imaging. In: Ashton, N., Lewis, S.G., Stringer, C. (Eds.), The Ancient Human Occupation of Britain, Amsterdam: The Netherlands, pp. 249–262.

Bello, S.M., Soligo, C., 2008. A new method for the quantitative analysis of cutmark micromorphology. J. Archaeol. Sci. 35, 1542–1552.

Bello, S.M., Parfitt, S.A., Stringer, C.B., 2009. Quantitative micromorphological analyses of cut marks produced by ancient and modern handaxes. J. Archaeol. Sci. 36, 1869–1880.

Bello, S.M., Parfitt, S.A., Stringer, C.B., 2011a. Earliest directly-dated human skull-cups. PLoS One 6 (2), e17026. http://dx.doi.org/10.1371/journal.pone.0017026.

Bello, S.M., Verveniotou, E., Cornish, L., Parfitt, S.A., 2011b. Dimensional microscope analysis of bone and tooth surface modifications: comparisons of fossil specimens and replicas. Scanning 33, 316–324.

Bello, S.M., De Groote, I., Delbarre, G., 2013a. Application of 3-dimensional microscopy and micro-CT scanning to the analysis of Magdalenian portable art on bone and antler. J. Archaeol. Sci. 40, 2464–2476.

Bello, S.M., Parfitt, S.A., Groote, I., Kennaway, G., 2013b. Investigating experimental knapping damage on an antler hammer: a pilot-study using high-resolution imaging and analytical techniques. J. Archaeol. Sci. 40, 4528–4537.

Bello, S.M., Saladié, P., Cáceres, I., Rodríguez-Hidalgo, A., Parfitt, S.A., 2015. Upper Palaeolithic ritualistic cannibalism: Gough's Cave (Somerset, UK) from head to toe. J. Hum. Evol. 82, 170–189.

Binford, L.R., 1981. Bones: Ancient Men, Modern Myths. Academic press, New York.

Bonney, H., 2014. An investigation of the use of discriminant analysis for the classification of blade edge type from cut Marks made by metal and bamboo blades. Am. J. Phys. Anthropol. 154, 575–584.

Boschin, F., Crezzini, J., 2012. Morphometrical analysis on cut marks using a 3D digital microscope. Int. J. Osteoarchaeol. 22, 549–562.

Bunn, H.T., 1982. Meat Eating and Human Evolution: Studies on the Diet and Subsistence Patterns of Plio-pleistocene Hominids in East Africa. Ph.D. dissertation. University of California, Berkeley.

Bunn, H.T., Kroll, E.M., 1986. Systematic butchery by Plio-Pleistocene hominid at 27 olduvai Gorge, Tanzania. Curr. Anthropol. 27, 431–452.

Capaldo, S.D., 1997. Experimental determinations of carcass proceding by Plio-Pleistocene hominids and carnivores at FLK 22 (Zinjanthropus), Olduvai Gorge, Tanzania. J. Hum. Evol. 33, 555–598.

Choi, K., Driwantoro, D., 2007. Shell tool use by early members of Homo erectus in Sangiran, central Java, Indonesia: cut mark evidence. J. Archaeol. Sci. 34, 48–58.

Core, R. Team, 2013. A Language and Environment for Statistical Computing. R Foundation for Statistical Computing, Vienna, Austria. URL. http://www.R-project.org/.

Crezzini, J., Boschin, F., Wierer, U., Boscato, P., 2014. Wild cats and cut marks: exploitation of *Felis silvestris* in the Mesolithic of Galgenbühel/Dos de la Forca (South Tyrol, Italy). Quat. Int. 330, 52–60.

De Juana, S., Galán, A.B., Domínguez-Rodrigo, M., 2010. Taphonomic identification of cut marks made with lithic handaxes: an experimental study. J. Archaeol. Sci. 37, 1841–1850.

Deseilligny, M.P., Clery, I., 2011. Apero, an open source bundle adjustment software for automatic calibration and orientation of set of images. In: Proceedings of the ISPRS Symposium, 3DARCH11, pp. 269–277.

Domínguez-Rodrigo, M., 1997. Meat eating by early homids at FLK Zinj 22 Site, Olduvay Gorge Tanzania: an experimental a roach using cut-mark data. J. Hum.

Evol. 33, 669–690.
Domínguez-Rodrigo, M., Barba, R., Egeland, C.P., 2007. Deconstructing Olduvai. Springer, New York.
Domínguez-Rodrigo, M., de Juana, S., Galán, A.B., Rodríguez, M., 2009. A new protocol to differentiate trampling marks from butchery cut marks. J. Archaeol. Sci. 36, 2643–2654.
During, E.M., Nilsson, L., 1991. Mechanical surface analysis of bone: a case study of cut marks and enamel hypoplasia on a Neolithic cranium from Sweden. Am. J. Phys. Anthropol. 84, 113–125.
Galán, A.B., Domínguez-Rodrigo, M., 2013. An experimental study of the anatomical distribution of cut marks created by filletng and disarticulation on the long bone ends. Archeometry 55 (6), 1132–1149.
Gilbert, W.H., Richards, G.D., 2000. Digital imaging of bone and tooth modification. Anat. Rec. 261, 237–246.
González-Aguilera, D., Guerrero, D., Hernández-López, D., Rodríguez-Gonzálvez, P., Pierrot, M., Fernández-Hernández, J., 2013. PW, Photogrammetry Workbench. http://www.isprs.org/catcon/catcon6.aspx (accessed 30.04.14).
Greenfield, H.J., 1999. The origins of metallurgy: distinguishing stone from metal cut-marks on bones from archaeological sites. J. Archaeol. Sci. 26, 797–808.
Greenfield, H.J., 2004. The butchered animal bone remains from Ashqelon, Afridar-Area G. Antiqot 45, 243–261.
Greenfield, H.J., 2006a. The butchered animal bones from Newe Yam, a submerged pottery Neolithic site off the Carmel Coast. J. Israel Prehist. Soc. 36, 173–200.
Greenfield, H.J., 2006b. Slicing cut marks on animal bones: diagnostics for identifying stone tool type and raw material. J. Field Archaeol. 31, 147–163.
Güth, A., 2012. Using 3D scanning in the investigation of Upper Palaeolithic engravings: results of a pilot study. J. Archaeol. Sci. 39 (10), 3105–3114.
Hartley, R., Zisserman, A., 2003. Multiple View Geometry in Computer Vision. Cambridge University Press.
Hillson, S., Parfitt, S.A., Bello, S.M., Roberts, M.B., Stringer, C.B., 2010. Two hominin incisor teeth from the Middle Pleistocene site of Boxgrove, Sussex, England. J. Hum. Evol. 59, 493–503.
Hirschmuller, H., 2005. Accurate and efficient stereo processing by semi-global matching and mutual information. In: IEEE Computer Society Conference on Computer Vision and Pattern Recognition. CVPR 2005, vol. 2, pp. 807–814.
Kaiser, T.M., Katterwe, H., 2001. The application of 3D-Microprofilometry as a tool in the surface diagnosis of fossil and sub-fossil vertebrate hard tissue. An example from the Pliocene Upper Laetoli Beds, Tanzania. Int. J. Osteoarchaeol. 11, 350–356.
Kraus, K., 1993. Photogr. Fundamentals Standard Processes, vol. 1. DummlersVerlag, Bonn, Germany, ISBN 3-427-78684-6.
Lartet, E., 1860. On the coexistence of man with certain extinct quadrupeds, proved by fossil bones from various Pleistocene deposits, bearing incisions made by sharp instruments. Q. J. Sociol. Soc. Lond. 16, 471–479.
Lartet, E., Christy, H., 1875. Reliquiae Acquitanicae Being Contributions to the Archaeology and Paleontology of Perigord and Adjoining Provinces of Southern France. Willians and Nagorte, London.
Lê, S., Josse, J., Husson, F., 2008. FactoMineR: an r package for multivariate analysis. J. Stat. Softw. 25 (1), 1–18.
Lewis, J.E., 2008. Identifying sword marks on bone: criteria for distinguishing between cut marks made by different classes of bladed weapons. J. Archaeol. Sci. 35, 2001–2008.
Longuet-Higgins, H.C., 1987. A computer algorithm for reconstructing a scene from two projections. In: Fischler, M.A., Firschein, O. (Eds.), Readings in Computer Vision: Issues, Problems, Principles, and Paradigms, pp. 61–62.
Lowe, D.G., 1999. Object recognition from local scale-invariant features. In: Proceedings of the 1999 IEEE International Conference on Computer Vision, Kerkyra, Greece, 20–27 September 1999, 2, pp. 1150–1157.
Lyman, R.L., 1987. Archaeofaunas and butchery studies: a taphonomic perspective. In: En Schiffer, M. (Ed.), Advances in Archaeological Method and Theory, vol. 10, pp. 249–337. New York.
Marín-Monfort, M.D., Pesquero, M.D., Fernández-Jalvo, Y., 2014. Compressive marks from gravel substrate on vertebrate remains: a preliminary experimental study. Quat. Int. 330 (30), 118–125.
Martin, H., 1909. Desarticulation des quelques regions chez les rumiants et le cheval a l'epoque mousterienne. Bull. Soc. Préhist. Franç. 7, 303–310.
Montani, I., Sapin, E., Sylvestre, R., Marquis, R., 2012. Analysis of Roman pottery graffiti by high resolution capture and 3D laser profilometry. J. Archaeol. Sci. 39 (11), 3349–3353.
Morel, J.M., Yu, G., 2009. Asift: a new framework for fully affine invariant image comparison. SIAM J. Imag. Sci. 2, 438–469.
Nilsen, P.J., 2001. An Actualistic Butchery Study in South Africa and its Implications for Reconstructing Hominid Strategies of Carcass Acquisition and Butchery in the Upper Pleistocene and Plio-pleistocene (Ph.D. dissertation). University of Cape Town.
Olsen, S.L., 1988. The Identification of Stone and Metal Tool Marks on Bone Artefact, vol. 452. BAR, pp. 337–360.
Peale, J., 1870. On the Uses of the Brain and Marrow of Animals Among the Indians of North America. Smithsonian Institution Annual Report for, 1870, pp. 390–391.
Rodríguez-Martin, M., Lagüela, S., González-Aguilera, D., Arias, P., 2015a. Cooling analysis of welded materials for crack detection using infrared thermography. Infrared Phys. Technol. 67, 547–554.
Rodríguez-Martin, M., Lagüela, S., González-Aguilera, D., Arias, P., 2015b. Procedure for quality inspection of welds based on macro-photogrammetric three-dimensional reconstruction. Opt. Laser Technol. 73, 54–62.
Schulting, R.J., Bello, S.M., Chandler, B., Higham, T.F.G., 2015. A cut-marked and fractured Mesolithic human bone from Kent's Cavern, Devon, UK. Int. J. Osteoarchaeol. 25 (1), 31–44.
Sherratt, E., 2014. Quick Guide to Geomorph v. 2.0. http://www.public.iastate.edu/~dcadams/PDFPubs/Quick%20Guide%20to%20Geomorph%20v2.0.pdf.
Shipman, P., 1981. Life Historia of a Fosil. An Introduction to Taphonomy and Paleoecology. Harvard University Press.
Shipman, P., Rose, J., 1983. Early hominid hunting, buchering and carcass-processing behaviours: a roaches to tha fosil record. J. Anthropol. Archaeol. 2, 57–98.
Smith, M.J., Brickley, M.B., 2004. Animals and interpretation of flint toolmarks found on bones from West Tump Long Barrow, Gloucestershire. Int. J. Osteoarchaeol. 14, 18–33.
Spennerman, D.H.R., 1990. Don't forget the bamboo on recognising and interpretating butchery narcks in tropical faunal assemblages some comments asking for cauting. In: Solomon, S., Davidson, I., Watson, D. (Eds.), Problems Solving Taphonomy Tempus 2, pp. 80–101.
Walker, P.L., 1978. Butchering and stone tool function. Am. Antiq. 43, 710–715.
West, J., Louys, J., 2007. Differentiating bamboo from stone tool cut marks in the zooarchaeological record, with a discussion on the use of bamboo knives. J. Archaeol. Sci. 34, 512–518.
White, T.E., 1952. Observations on the butchering technique of some aboriginal peoples, 1. Am. Antiq. 17, 337–338.
White, T.E., 1953. Observations on the butchering technique of some aboriginal peoples, 2. Am. Antiq. 19, 160–164.
White, T.E., 1954. Observations on the butchering technique of some aboriginal peoples, 3, 4, 5, 6. Am. Antiq. 19, 254–264.
White, T.E., 1955. Observations on the butchering technique of some aboriginal peoples, 7, 8, 9. Am. Antiq. 21, 170–178.
Yravedra, J., Morín, J., Agustí, E., Sanabria, P., López, M., Urbina, D., López-Frailes, F.J., López, G., Illán, J., 2009. Implicaciones Metalúrgicas de las marcas de corte en la transición Bronce Final-Hierro en el interior de la Península Ibérica.
Zelditch, M.L., Swiderski, D.L., Sheets, H.D., 2012. Geometric Morphometrics for Biologists. Academic Press.